

# A theoretical investigation provides an integrated understanding of the complex regulatory network controlling *Arabidopsis* root hair patterning.

## Author list

Hayley Mills<sup>1</sup>, George Janes<sup>2</sup>, Anthony Bishopp<sup>2</sup>, Natasha Savage<sup>1\*</sup>

<sup>1</sup>Institute of Systems, Molecular and Integrative Biology. University of Liverpool. UK.

<sup>2</sup>School of Biosciences. University of Nottingham. UK.

\*nsavage@liverpool.ac.uk

## Abstract

A complex regulatory network controlling *Arabidopsis* root hair patterning has been defined using data collected over decades by numerous labs. The network, embedded in the root epidermis, contains positive and negative feedback loops, undergoes cell-cell signalling within the epidermal tissue, and receives positional signalling from underlying tissue. While there are extensive data regarding individual components and their interactions within the network, the sufficiency of the regulatory network to produce robust epidermal patterning is not clear, nor is it clear how individual components and interactions work together to ensure correct epidermal patterning. Mathematical modelling was used to address the questions of sufficiency, and to gain an integrated understanding of collective behaviour emerging from individual components and interactions within the regulatory network.

Theoretical experiments were performed on a model of the *Arabidopsis* root hair patterning regulatory network. It was found that our current understanding of the epidermal patterning regulatory network was insufficient to reproduce experimental data. The model was used to hypothesise the existence of an additional negative feedback loop which, when added to the currently understood regulatory network, enabled the model to reproduce both wild type and mutant root hair patterning. Results of theoretical experiments on the modified regulatory network were used to; define an essential relationship between the diffusive movement of two cell-cell signalling proteins; show that directed movement dysregulation of another cell-cell signalling protein causes root hair patterning to appear as though it no longer receives positional cues; and show that cooperativity or oligomerisation within the regulatory network's positive feedback loop are essential.

This work presents an in-depth, integrated, exploration of the regulatory network controlling epidermal root hair patterning in *Arabidopsis*, and derives new insight into the roles of network components, and their combined mechanistic action.

## 1 Introduction.

The collective knowledge regarding the regulation of a process within a biological system is often mapped onto a regulatory network. Practical constraints often lead to individual groups focussing on certain aspects of a regulatory network, resulting in subsets of network components and their interactions being studied in isolation from the rest of the network. Mathematical modelling is a tool with which one can integrate the distributed data generated by numerous groups, over many years. The resulting regulatory network model can be used to understand how network components work together to control the processes under scrutiny.

This study uses mathematical modelling to bring together the vast body of work which has uncovered components, and regulatory links, within the network responsible for *Arabidopsis* root epidermal patterning. While the components and interactions within the *Arabidopsis* root epidermal patterning network are well studied in isolation, their integrated ability to produce epidermal patterns is not clear. Here, a mathematical model of the *Arabidopsis* regulatory network was built, using published data, and used to address the question of sufficiency of our current knowledge to reproduce epidermal patterning. The model was also used



There remains an open question regarding additional regulation on *WER* transcription. A modelling study showed that *WER* regulation, in addition to the cortical signal, was necessary for the modelled root epidermis to reproduce biological data, and suggested that *WER* transcription may be repressed by CPC [12]. However, the model in [12] was a probabilistic Boolean model which predated the discovery of MYB23 [5] and modelled SCM in its old role, as a cortical signal receptor [16]. An experimental study presented the hypothesis that there was no additional regulation on *WER*, that competitive binding of GL3/EGL3 by *WER* and CPC was sufficient to enable epidermal patterning [9]. The question of *WER* transcriptional regulation was addressed in this study. Here it was found that additional *WER* transcriptional regulation was necessary for correct epidermal patterning and a regulation mechanism was proposed.

CPC can move between epidermal cells and data suggests that this movement has a regulatory component [17]. Recently it has been shown that SCM facilitates the movement of CPC by importing CPC into the cell [11]. SCM has been shown to be preferentially expressed in trichoblast cells, in the H position [18], and so SCM imports CPC into trichoblast cells from neighbouring atrichoblast cells. CPC translation is promoted in atrichoblast cells by the *WER*/MYB23 complex [14,15], wherein the resulting CPC protein competes with *WER* and MYB23 for GL3 and EGL3 binding. It seems likely then, that the directed removal of CPC, by SCM, from atrichoblast cells would promote correct epidermal patterning. In this study it is shown that SCM import of CPC decreases the differentiating epidermal cells' sensitivity to changes in reaction rates, making correct patterning more robust.

SCM was initially thought to be a cortical signal receptor because trichoblast cells became decoupled from the cortical cleft in *scm* mutants [16]. Now SCM's role has been redefined as a CPC importer [11], it is not clear that without any change to the epidermal cells' ability to perceive the cortical signal, removing CPC import would result in the *scm* mutant trichoblast, atrichoblast pattern. Within this study it is shown that the removal of CPC import alone is sufficient to account for the *scm* mutant pattern, the *scm* pattern can be reproduced without any change to the epidermal cells' ability to perceive the cortical signal.

GL3 can also move between epidermal cells [13] as can EGL3, although EGL3 movement has been reported to be restricted when compared to the movement of GL3 [19]. GL3, EGL3 movement between cells is hypothesised to be diffusive [12,20]. The *WER*/MYB23 complex represses GL3, EGL3 transcription enabling GL3, EGL3 concentration gradients which facilitate the diffusive movement of GL3, EGL3 from trichoblast cells to atrichoblast cells, wherein GL3, EGL3 become available to form the *WER*/MYB23 or CPC complex. It is not known what, if any, functional role the restriction of EGL3 movement has in epidermal patterning. In this study the necessity of EGL3 restricted movement is investigated and found to be essential for correct epidermal patterning. It is shown that EGL3 restricted movement, coupled with differential binding affinities during *WER*/MYB23 and CPC complex formation promote correct epidermal patterning.

Multiple binding sites have been reported on three reactions within the regulatory network, two of which appear within the MYB23 positive feedback loop. There are multiple binding for *WER* on the *MYB23* promoter [5], *WER* on the *CPC* promoter [14,15], and multiple GL3, EGL3, *WER*, MYB23 proteins are reported to be involved in *WER*/MYB23 complex formation [9]. Cooperativity and oligomerisation impact reaction dynamics, producing reaction insensitivity at low concentrations of the reactants and nonlinear reaction rate increases as reactant concentrations increase. This study shows that at least one multiple binding site reaction within the MYB23 positive feedback loop is essential for correct patterning, and suggests that the roles of multiple binding site reactions within the MYB23 positive feedback loop are to protect the regulatory network from noise driven patterning early in development, and to create switch like dynamics later in development as regulator concentrations increase.

These results present an in-depth, integrated, understanding of the regulatory network controlling *Arabidopsis* root hair patterning.

## 2 Materials and Methods.

### 2.1 Model Equations

Terms within the differential equations were derived using either mass action kinetics or the Hill equation [21].

#### **GL3, EGL3**

The dynamics of *GL3*, denoted  $g$ , and *EGL3*, denoted  $e$ , are governed by basal transcription at rates  $b_g$  and  $b_e$  respectively, degradation at rates  $d_g$  and  $d_e$ , and repression of *GL3*, *EGL3* transcription by the total concentration of WER/MYB23 complex [13,5], denoted  $A_T$ , Equation (18). The repression of *GL3*, *EGL3* transcription by the total WER/MYB23 complex has been modelled as a *GL3*, *EGL3* degradation term with degradation rates  $r_g$ ,  $r_e$ , respectively.

$$\frac{d}{dt}g = b_g - r_g A_T g - d_g g \quad (1)$$

$$\frac{d}{dt}e = b_e - r_e A_T e - d_e e \quad (2)$$

#### **GL3, EGL3**

*GL3*, denoted  $G$ , and *EGL3*, denoted  $E$ , diffuse between epidermal cells [13,19]. Diffusion is described using the standard Laplacian operator,  $\Delta$ , with diffusion coefficients  $D_G$  for *GL3* and  $D_E$  for *EGL3*. *GL3*, *EGL3* translation takes place with rates  $q_G$  and  $q_E$ , respectively. *GL3*, *EGL3* degradation takes place with rates  $d_G$  and  $d_E$ . Other reactions to affect the dynamics of *GL3*, *EGL3* are those involved in WER/MYB23 complex and CPC complex formation and deformation [6,9]. It has been proposed that the WER/MYB23 complex contains at least two *GL3*/*EGL3* and WER/MYB23 proteins [9]. To enable the effect of the number of *GL3*/*EGL3* and WER/MYB23 proteins within the WER/MYB23 complex to be investigated, their number was chosen from a finite set of possibilities;  $n_1 \in \{1,2,3,4\}$  for *GL3*, *EGL3* and  $n_2 \in \{1,2,3,4\}$  for WER, MYB23. Thus,  $n_1 \in \{1,2,3,4\}$  *GL3*, *EGL3* proteins are lost to WER/MYB23 complex formation and returned to the *GL3*, *EGL3* pool on WER/MYB23 complex deformation. Because of lack of evidence to the contrary, one *GL3*, *EGL3* protein is lost to CPC complex formation and returned on CPC complex deformation.  $W$  denotes WER,  $M$  denotes MYB23 and  $C$  denotes CPC.  $A_{GW}$  represents the WER complex containing *GL3*,  $A_{GM}$  represents the MYB23 complex containing *GL3*,  $A_{EW}$  represents the WER complex containing *EGL3*, and  $A_{EM}$  represents the MYB23 complex containing *EGL3*.  $I_{GC}$  and  $I_{EC}$  denote the CPC complexes containing *GL3* and *EGL3* respectively.  $k_{11}$  to  $k_{18}$  are reaction rates for WER/MYB23 complex formation and deformation,  $k_{21}$  to  $k_{24}$  are reaction rates for CPC complex formation and deformation.

$$\frac{\partial}{\partial t}G = q_G g - n_1 G^{n_1} (k_{11} W^{n_2} + k_{15} M^{n_2}) + n_1 (k_{12} A_{GW} + k_{16} A_{GM}) - k_{21} GC + k_{22} I_{GC} - d_G G + D_G \Delta G \quad (3)$$

$$\frac{\partial}{\partial t}E = q_E e - n_1 E^{n_1} (k_{13} W^{n_2} + k_{17} M^{n_2}) + n_1 (k_{14} A_{EW} + k_{18} A_{EM}) - k_{23} EC + k_{24} I_{EC} - d_E E + D_E \Delta E \quad (4)$$

#### **WER**

*WER* concentration, denoted  $w$ , is increased by basal transcription, rate  $b_w$ . *WER* transcription is repressed by a cortical signal [3], denoted  $X$ ,  $X \in \{0,1\}$ .  $X = 1$  when the epidermal cell lies over a cortical cleft,  $X = 0$  otherwise. It is hypothesised that the cortical signal was received by a receptor on the epidermal cell. Previous studies had proposed this receptor was SCM, as trichoblast cell fate was decoupled from the cortical cleft in roots without SCM [16]. Recently, the role of SCM in *WER* transcriptional regulation has been brought into question and data suggests that SCM functions to aid the movement of CPC between epidermal cells [11]. Nonetheless, positional signalling is still thought to be received by the epidermal cells. Thus, the model contains an unidentified cortical signal receptor,  $R_X$ . A previous modelling study suggested that *WER* transcription may be also be repressed by CPC [12]. Also investigated in this study is the repression of *WER* transcription by the total concentration of CPC complex, denoted  $I_T$ , see Equation (19). Repression of *WER* transcription is modelled as *WER* degradation,  $r_{w21}$  is the rate at which the cortical signal represses *WER* via  $R_X$ , and rates  $r_{w11}$ ,  $r_{w12}$  are for the repression of *WER* by CPC and total CPC complex. *WER* has basal degradation rate  $d_w$ .

$$\frac{d}{dt}w = b_w - X(r_{w21} R_X)w - (r_{w11} C + r_{w12} I_T + d_w)w \quad (5)$$

## MYB23

*MYB23*, denoted  $m$ , transcription is promoted by total WER/MYB23 complex,  $A_T$ . There are four WER binding sites in the *MYB23* promoter, one appearing to have a more important role than the other three [5]. Thus, the number of WER/MYB23 complexes needed for *MYB23* transcription,  $n_3$ , was investigated,  $n_3 \in \{1,2,3,4\}$ . The mass action kinetics term to describe the total WER/MYB23 complex promotion of *MYB23* transcription was,  $p_m A_T^{n_3}$ , where  $p_m$  is the transcription rate. It was found that using mass action kinetics for transcriptional promotion resulted in an unlikely *MYB23* concentration amplification for  $n_3 > 1$ , data not shown. Thus, the Hill equation [21], rather than mass action kinetics, was used to describe total WER/MYB23 complex promotion of *MYB23* transcription. The Hill coefficient is a measure of cooperativity between binding sites, with a maximum value equalling the number of available binding sites [22]. Thus, the Hill coefficient for *MYB23* transcriptional was set to  $n_3 \in \{1,2,3,4\}$ . The maximum rate of *MYB23* transcription was denoted  $p_m$ .  $K_m$  represents dissociation constant, as derived by mass action kinetics.

$$\frac{d}{dt}m = p_m \frac{A_T^{n_3}}{K_m + A_T^{n_3}} - d_m m \quad (6)$$

## WER, MYB23

WER, MYB23 translation takes place with rates  $q_W$  and  $q_M$ , and degradation with rates  $d_W$  and  $d_M$ , respectively.  $n_2 \in \{1,2,3,4\}$  WER and MYB23 proteins are lost to the formation of a WER/MYB23 complex and gained when a WER/MYB23 complex disassociates [9].

$$\frac{d}{dt}W = q_W W - n_2 W^{n_2} (k_{11} G^{n_1} + k_{13} E^{n_1}) + n_2 (k_{12} A_{GW} + k_{14} A_{EW}) - d_W W \quad (7)$$

$$\frac{d}{dt}M = q_M M - n_2 M^{n_2} (k_{15} G^{n_1} + k_{17} E^{n_1}) + n_2 (k_{18} A_{EM} + k_{16} A_{GM}) - d_M M \quad (8)$$

## CPC

*CPC*, denoted  $c$ , transcription is promoted by total WER/MYB23 complex [14,15]. Three distinct WER binding sites have been found on the *CPC* promotor, each with different affinities to WER but all were required for proper gene expression [14,15]. Thus, the number of WER/MYB23 complex needed to promote *CPC* transcription was chosen from the set  $n_4 \in \{1,2,3\}$ . To prevent a biologically unlikely *CPC* concentration amplification caused by using mass action kinetics to describe total WER/MYB23 complex promotion of *CPC* transcription (data not shown), the Hill equation [21] was used, with Hill coefficient  $n_4 \in \{1,2,3\}$ . The maximum rate of *CPC* transcription was denoted  $p_c$  and  $K_c$  represents the dissociation constant.

$$\frac{d}{dt}c = p_c \frac{A_T^{n_4}}{K_c + A_T^{n_4}} - d_c c \quad (9)$$

## CPC

*CPC* translation rate was denoted  $q_C$ , and degradation rate denoted  $d_C$ . *CPC* concentration is increased when the *CPC* complex disassociates and decreased when it is formed [6,9]. *CPC* can move between epidermal cells [17]. Data suggests that SCM, denoted  $S$ , acts to facilitate the import of *CPC* [11]. The movement of *CPC* was described by two terms diffusion, with diffusion coefficient  $D_C$ , and SCM import, with proportionality constant  $\tilde{D}_C$ . *CPC* diffusion was calculated using the Laplacian operator and SCM import was calculated using a finite difference scheme,  $i$  is the epidermal cell index,  $C_i$  is the concentration of *CPC* in cell  $i$ ,  $S_i$  the concentration of SCM in cell  $i$ , Equation (11). As SCM has been shown to localise in cells in the H position [18], SCM  $S_i = 1$  when the epidermal cell lies over a cortical cleft, 0 otherwise.

$$\frac{\partial}{\partial t}C = q_C C + k_{22} I_{GC} + k_{24} I_{EC} - (k_{21} GC + k_{23} EC) - d_C C + \tilde{D}_C f(C, S) + D_C \Delta C \quad (10)$$

$$f(C, S) = (S_i(C_{i+1} + C_{i-1}) - C_i(S_{i+1} + S_{i-1})) \quad (11)$$

## WER/MYB23 complex

$$\frac{d}{dt}A_{GW} = k_{11} G^{n_1} W^{n_2} - k_{12} A_{GW} \quad (12)$$

$$\frac{d}{dt}A_{EW} = k_{13} E^{n_1} W^{n_2} - k_{14} A_{EW} \quad (13)$$

$$\frac{d}{dt}A_{GM} = k_{15}G^{n_1}M^{n_2} - k_{16}A_{GM} \quad (14)$$

$$\frac{d}{dt}A_{EM} = k_{17}E^{n_1}M^{n_2} - k_{18}A_{EM} \quad (15)$$

### CPC complex

$$\frac{d}{dt}I_{GC} = k_{21}GC - k_{22}I_{GC} \quad (16)$$

$$\frac{d}{dt}I_{EC} = k_{23}EC - k_{24}I_{EC} \quad (17)$$

### Total WER/MYB23 and CPC complexes

As MYB23 can functionally replace WER [5] and GL3, EGL3 are functionally similar [6,13,23] total WER/MYB23 complex was used within the relevant differential equations, Equation (18). Similarly, for the CPC complexes and total CPC complex was used, Equation (19).

$$A_T = A_{GW} + A_{EW} + A_{GM} + A_{EM} \quad (18)$$

$$I_T = I_{GC} + I_{EC} \quad (19)$$

## 2.2 Parameter Search

There are a lack of data measuring the rates of reactions within the regulatory network controlling *Arabidopsis* root epidermal patterning. A random search approach was chosen to explore the ability of the model to reproduce biological data.

Thirty-eight core parameters were defined, Table 1. These parameters were rates for reactions which remained unchanged for all modelling investigations. A core parameter set was defined as thirty-eight parameter values, one for each core parameter. 20,000 core parameter sets were chosen uniformly at random from the arbitrary interval (0,10]. Core parameter sets were indexed 1 to 20,000 and fixed. The values of thirteen additional parameters were set depending on the mechanistic investigation being undertaken, Table 2.

**Table 1. Core parameters.** Core parameter names, descriptions and intervals from which core parameter values were chosen. 20,000 core parameter sets were chosen uniformly at random from the interval (0,10].  $j$  is an index used to identify each core parameter during univariate sensitivity analysis (Section 2.3).

$j$		<b>WER/MYB23 complex formation and deformation</b>	
1	$k_{11}$	$A_{GW}$ association	(0,10]
2	$k_{12}$	$A_{GW}$ disassociation	(0,10]
3	$k_{13}$	$A_{EW}$ association	(0,10]
4	$k_{14}$	$A_{EW}$ disassociation	(0,10]
5	$k_{15}$	$A_{GM}$ association	(0,10]
6	$k_{16}$	$A_{GM}$ disassociation	(0,10]
7	$k_{17}$	$A_{EM}$ association	(0,10]
8	$k_{18}$	$A_{EM}$ disassociation	(0,10]
<b>CPC complex formation and deformation</b>			
9	$k_{21}$	$I_{GC}$ association	(0,10]
10	$k_{22}$	$I_{GC}$ disassociation	(0,10]
11	$k_{23}$	$I_{EC}$ association	(0,10]
12	$k_{24}$	$I_{EC}$ disassociation	(0,10]
<b>basal degradation</b>			
18	$d_G$	GL3 protein	(0,10]
19	$d_E$	EGL3 protein	(0,10]
20	$d_C$	CPC protein	(0,10]
21	$d_W$	WER protein	(0,10]
22	$d_M$	MYB23 protein	(0,10]
23	$d_g$	GL3 mRNA	(0,10]
24	$d_e$	EGL3 mRNA	(0,10]
25	$d_c$	CPC mRNA	(0,10]
26	$d_w$	WER mRNA	(0,10]
27	$d_m$	MYB23 mRNA	(0,10]

$j$		<b>basal transcription</b>	
15	$b_g$	GL3 mRNA	(0,10]
16	$b_e$	EGL3 mRNA	(0,10]
17	$b_w$	WER mRNA	(0,10]
<b>maximum transcription rate</b>			
33	$p_c$	CPC mRNA	(0,10]
34	$p_m$	MYB23 mRNA	(0,10]
<b>disassociation constant</b>			
38	$K_c$	WER on CPC transcript	(0,10]
37	$K_m$	WER on MYB23 transcript	(0,10]
<b>transcriptional repression</b>			
35	$r_g$	GL3 by WER/MYB23 complex	(0,10]
36	$r_e$	EGL3 by WER/MYB23 complex	(0,10]
<b>translation</b>			
28	$q_G$	GL3 protein	(0,10]
29	$q_E$	EGL3 protein	(0,10]
30	$q_C$	CPC protein	(0,10]
31	$q_W$	WER protein	(0,10]
32	$q_M$	MYB23 protein	(0,10]
<b>protein movement</b>			
13	$D_G$	GL3 diffusion	(0,10]
14	$D_C$	CPC diffusion	(0,10]

**Table 2. Parameters changed during mechanistic investigations.** Parameter names, descriptions and intervals from which parameter values were chosen. Parameters were set depending on the mechanistic investigation being undertaken. Descriptions of mechanistic investigations are given in the sections indicated at the top of each parameter column. For each of the 20,000 core parameter sets, the parameters  $n_1$ ,  $n_2$ ,  $n_3$  and  $n_4$  were either chosen uniformly at random from the set shown. When parameter intervals are given the parameter was chosen uniformly at random from the interval, for each of the 20,000 core parameter sets.

		§ 3.1	§ 3.4	§ 3.5
	<b>number of proteins in WER/MYB23 complex</b>			
$n_1$	GL3, EGL3	{2,3,4}	Table 7.	{2,3,4}
$n_2$	WER, MYB23	{2,3,4}	Table 7.	{2,3,4}
	<b>number of binding sites on transcript</b>			
$n_3$	WER on <i>MYB23</i>	{2,3,4}	Table 7.	{2,3,4}
$n_4$	WER on <i>CPC</i>	{2,3}	Table 7.	{2,3}
	<b>WER transcriptional repression</b>			
$r_{w11}$	by <i>CPC</i>	Table 5.	Table 5.	Table 5.
$r_{w12}$	by <i>CPC</i> complex	Table 5.	Table 5.	Table 5.
	<b>EGL3 movement</b>			
$D_E$	diffusion	0	0	(0,10]
	<b>SCM function</b>			
$S$	SCM as <i>CPC</i> importer	1, SCM+ 0, SCM-	1, SCM+ 0, SCM-	1, SCM+ 0, SCM-
$\tilde{D}_C$	<i>CPC</i> import via SCM	(0,10], SCM+ 0, SCM-	(0,10], SCM+ 0, SCM-	(0,10], SCM+ 0, SCM-
$R_X$	unknown receptor	(0,0.25]	(0,0.25]	(0,0.25]
$r_{w21}$	<i>WER</i> repression via $R_X$	(0,10]	(0,10]	(0,10]

Steady state solutions of models which included SCM, referred to as SCM+ models, were compared to wild type (WT) data. Steady state solutions of models which did not include SCM, referred to as SCM- models, were compared to *scm* mutant data. Biological data regarding the location of transcript and proteins are imaging data. Thus, the data indicates the total proteins in a cell, not whether those proteins are in a complex or not. For SCM+ model solutions, *in-silico* trichoblast cells were defined as having a steady state solution with high concentrations of total *CPC* [17], *GL3*, *EGL3*, total *EGL3* [6,19] and low concentrations of total *GL3* [13], *WER*, total *WER* [4], *MYB* and total *MYB* [5], when compared to atrichoblast cells. *In-silico* atrichoblast cells were defined as having a steady state solution with high concentrations of total *GL3*, *WER*, total *WER*, *MYB* and total *MYB*, and low concentrations of, total *CPC*, *GL3*, *EGL3*, total *EGL3* when compared to trichoblast cells, Figure 1B. A threshold was applied such that, for a concentration difference between the two cells to be considered significant the difference had to be over 10%.

For WT data trichoblast cells generally form single files over the cortical cleft, thus it can be assumed that regulatory network components which have this pattern are co-localised in the trichoblast cell. A similar argument can be made for atrichoblast regulatory network components. As cell fate is decoupled from the cortical cleft in *scm* mutant roots, regulatory network component co-localisation cannot be assumed. For SCM- model solutions the *in-silico* WER/MYB complex (used as a *GL2* proxy), total *WER* and *CPC* were compared to positional data for various trichoblast, atrichoblast markers [16,10,9,24,11,25].

A parameter set was labelled successful if both the steady state solutions of the SCM+ model could reproduce WT data and steady state solutions of the SCM- model could reproduce *scm* mutant data, Table 3. The WT data in Table 3 was generated by analysing twenty-three images of root cross-sections containing a *GL2* reporter, Figure 2A. *scm* mutant data was taken from publications. Trichoblast, atrichoblast, positional data was available in table form [10,9,24,11,25] however, the standard deviations in the published tables were much smaller than those calculated using model solutions and analysing published images. Thus, *scm* mutant data was calculated from eleven figures within six publications [16,10,9,24,11,25], Table 3 (supplementary information). The means calculated using the published imaging data were comparable to the published tabulated means.



**Table 3. WT and *scm* mutant cell type and position data.** Percentage of each epidermal cell type in the H and N positions.

	H position		N position	
	trichoblast	atrachoblast	trichoblast	atrachoblast
<b>WT</b>	93.7 ± 8.4	6.3 ± 8.4	1.2 ± 3.0	98.8 ± 3.0
<b><i>scm</i></b>	61.8 ± 12.9	38.2 ± 12.9	22.4 ± 15.2	77.6 ± 15.2

The parameter test protocol for each of the 20,000 core parameter sets, for each mechanistic combination under investigation, had three steps. Consider an arbitrary parameter set,  $P_i$ , where  $P_i$  is a list of parameter values for each of the parameters shown in Tables 1 and 2. Recall, a parameter set was labelled successful if both the steady state solutions of the SCM+ model could reproduce WT data and steady state solutions of the SCM- model could reproduce *scm* mutant data, Table 3. The SCM and cortical signal receptor parameter values for the three parameter test steps are shown in Table 4.

Step 1: Solve the SCM+ model with zero initial conditions, using parameter set  $P_i$ . If the solution of the SCM+ model, with zero initial conditions and  $P_i$ , was such that all *in-silico* trichoblast cells were in the H position and all *in-silico* atrichoblast cells were in the N position then parameter set  $P_i$  was used in step 2. Otherwise,  $P_i$  was considered unsuccessful and discarded.

Step 2: Create the SCM- model and attempt to fit model solutions to *scm* mutant data, Table 3. Although trichoblast cells were decoupled from the cortical cleft in *scm* mutant roots, trichoblast cells remained more likely to occupy the H position than atrichoblast cells, Table 3, leading to the suggestion of other, unidentified, cortical signal receptors [10]. *In-silico* cortical signal receptor strength was set within the interval (0,0.25], Table 4. The Cell type position data has a mean and standard deviation. To generate model solutions which enable comparison between *in-silico* and *in-planta* data, the SCM- model was solved twenty times with twenty sets of random initial conditions, for each parameter set  $P_i$ . The random initial conditions were such that, every component of the model, whose dynamics were described by a differential equation, was assigned an initial concentration,  $C_0$ , chosen uniformly at random from a given interval,  $C_0 = (0, C_{0_{max}}]$ ,  $C_{0_{max}} \leq 1$ . An attempt to fit the SCM- model to the data was made by changing the cortical signal receptor strength,  $R_x$ , and random initial conditions interval maximum,  $C_{0_{max}}$ . For each attempted fit, twenty SCM- solutions were generated and compared to *scm* mutant data, Table 3, using Welch's t-test. If the comparison resulted in a p-value greater than 0.05 then *in-silico* and *in-planta* data were not significantly different and parameter set  $P_i$  was labelled as a successful parameter set. If no successful fit could be found, parameter set  $P_i$  was considered unsuccessful and discarded. If a successful fit was found, parameter set  $P_i$  was used in step 3.

Step 3: Solve the SCM+ model with random initial conditions and receptor strength, fitted using the SCM- model, and compare solutions to data. The SCM+ model was solved twenty times and compared to WT data, Table 3, using Welch's t-test. If the comparison resulted in a p-value greater than 0.05 then *in-silico* and *in-planta* data were not significantly different and parameter set  $P_i$  was labelled as a successful parameter set.

**Table 4. SCM and cortical signal receptor parameter values for the three parameter test steps.**

	initial conditions	SCM, $S$	receptor, $R_x$
Step 1: SCM+	zero	1	1
Step 2: fit SCM-	random = (0,1]	0	(0,0.25]
Step 3: SCM+	random = (0,1]	1	(0,0.25]

## 2.3 Univariate Sensitivity Analysis

Univariate sensitivity analysis protocol. Let univariate sensitivity analysis be performed on successful parameter set  $P_i$ . The values of each of the core parameters, labelled  $j = \{1,2, \dots, 38\}$ , Table 1, within  $P_i$ , were changed one by one. The mechanistic parameters within  $P_i$ , Table 2, were not changed during sensitivity analysis, as those parameters define specific mechanisms under scrutiny and to change them would be to change the mechanism. Consider core parameter  $p_{i,j}$ , the value of  $p_{i,j}$  was multiplied by  $10^x$ , for  $x = \{-2, -1.75, -1.5, \dots, 2\}$  to give the perturbed parameter  $p'_{i,j}$ . For each perturbed parameter,  $p'_{i,j}$ , the SCM+ and SCM- models were solved twenty times, each with different noisy initial conditions. The model solutions were then compared with experimental data, Table 3. The success or fail of the model solution, solved with parameter set  $P_i$  containing the perturbed parameter  $p'_{i,j}$ , was recorded. An insensitive region for parameter

$p'_{i,j}$  was defined as  $r_{i,j} = x_{max} - x_{min}$ , where  $x_{min}$  was the minimum value of  $x$  for which the model solved with parameter set  $P_i$ , containing the perturbed parameter  $p'_{i,j}$ , matched the data, and  $x_{max}$  was the maximum value of  $x$  for which the model solved with parameter set  $P_i$ , containing the perturbed parameter  $p'_{i,j}$ , matched the data.

## 2.4 Experimental Methods

### Plant Materials

Wildtype *Arabidopsis* (Col-0) and *scm-2* mutants (SALK\_086357) were obtained from the Nottingham *Arabidopsis* stock centre (NASC). Sterile seeds were sown onto 1% agar plates containing 0.5x Murashige and Skoog salts at pH 5.7. Plates were then stratified at 4°C for 48h before being moved to growth rooms set at 21°C and a 16 hour day length.

### Molecular cloning and plant transformation

*Arabidopsis thaliana* *GLABRA2* (AT1G79840) genomic coding sequence was cloned from genomic DNA using primers designed according to the Greengate cloning system protocol (supplemental Table [26]). The *GLABRA2* coding sequence was cloned with a silent site-directed mutagenesis (V438V) to remove an internal Bsal site. mTurquoise was cloned from an existing plasmid with primers which include a glycine-serine (Gly-Ser) linker (GSSGGGSGGGGS) at the N-terminal end. The *GL2* promoter was cloned and described previously [27]. Restriction and ligation reactions were performed using Bsal and T4 DNA ligase (New England Biolabs, MA, USA). All entry plasmids were confirmed for presence of an insert by colony PCR and Sanger or Oxford Nanopore sequencing (Source Bioscience, Cambridge, UK). The entry vectors were used to generate an expression vector with *GL2* fused with mTurquoise at the C-terminus under the control of *GL2* promoter (supplemental figure). Other components of the construct were derived from the Greengate kit described by Lampropoulos *et al.* (2013). This kit is available from Addgene (Kit #1000000036). The construct was assembled in the pGGZ001 Greengate destination vector (supplemental figure). Greengate assembly reactions were performed using NEB Golden Gate Cloning Kit (New England Biolabs, MA, USA). Final expression constructs were confirmed by colony PCR, restriction digest and Oxford Nanopore sequencing.

The expression vector was transformed into *Agrobacterium tumefaciens* by electroporation transformation in combination with pSOUP, which is necessary for proper replication of the pGREEN-based plasmid. *A. tumefaciens* colonies were selected using colony PCR for presence of the expression vector. These were cultured and then used to transform *Arabidopsis thaliana* plants via the floral dip method [28]. The construct was transformed into Columbia 0 background and *scm-2* (SALK\_086357; insertion at *SCRAMBLED/STRUBBELLIG* AT1G11130; [16]). Transformant plants were selected for using hygromycin resistance.

### Imaging and image processing

5-day old seedlings were fixed with 4% paraformaldehyde in phosphate-buffered saline pH7.4 and cleared according to the Clearsee method [29], staining for 1h with Direct Red 23 (Sigma Aldrich) during clearing as described by Ursache *et al.* (2018) [30]. After clearing the root tips were mounted on slides and imaged on a Leica SP8 confocal microscope. Direct red 23 was excited using a 561nm laser line and detected at 580-615nm. mTurquoise was excited using a 442nm laser line and detected at 450-518nm. Data was processed using FIJI (ImageJ) and cell identity counts based on presence or absence of *GLABRA2* protein estimated by mTurquoise signal.

## 3 Results.

### 3.1 The regulatory network model can reproduce WT and *scm* epidermal patterning if repression of *WER* is colocalised with the CPC complex.

To understand if the most up to date published reactions were sufficient to enable *in-silico* trichoblast patterning that matched biological data, the mechanistic parameters shown in Table 2 were set such that the equations modelled; SCM as a CPC importer, EGL3 restricted movement, cooperativity on *MYB23* and *CPC* transcription and oligomerisation within the *WER*/*MYB23* complex. *WER* transcription is directly repressed by the cortical signal. If *WER* transcription is also directly repressed by components of the regulatory network

is not clear. A previous modelling study suggested that *WER* transcription may be also be repressed by CPC [12]. The model in [12] was a probabilistic Boolean model which predated the discovery of MYB23 and modelled SCM as a cortical signal receptor, as was the theory at the time. An experimental study presented the hypothesis that competitive binding of GL3/EGL3 by *WER* and CPC was sufficient to enable epidermal patterning [9]. Both published mechanisms were investigated using the model, Table 2, column §3.1, Table 5. The different forms of the equation describing *WER* concentration dynamics, Equation (5), are shown in Table 6. None of the 20,000 core parameter sets could reproduce the biological data, for either of the mechanisms. Thus, competitive binding alone is insufficient to enable *Arabidopsis* root epidermal patterning. *WER* transcriptional repression by CPC was also inadequate to enforce the correct patterning *in-silico*. This is perhaps unsurprising as *CPC* translation is promoted by the *WER*/MYB23 complex and *CPC* translation is colocalised with the *WER*/MYB23 complex. Thus, when unbound *CPC* repressed *WER* translation it hindered the ability of the *WER*/MYB23 complex to become dominant.

**Table 5. Mechanistic parameter intervals for *WER* transcriptional repression investigation.** CS stands for cortical signal. Other parameter intervals are shown in Tables 1 and 2.

parameter descriptions		parameter values for each mechanism		
	<b>WER transcriptional repression</b>	<b>CS only</b>	<b>CS &amp; CPC</b>	<b>CS &amp; CPC complex</b>
$r_{w11}$	by CPC	0	(0,10]	0
$r_{w12}$	by CPC complex	0	0	(0,10]

**Table 6. Forms of Equation (5).**

Equation (5)	
General form	$\frac{d}{dt}w = b_w - X(r_{w21}R_X)w - (r_{w11}C + r_{w12}I_T + d_w)w$
<b>CS only</b>	$\frac{d}{dt}w = b_w - X(r_{w21}R_X)w - d_w w$
<b>CS &amp; CPC</b>	$\frac{d}{dt}w = b_w - X(r_{w21}R_X)w - (r_{w11}C + d_w)w$
<b>CS &amp; CPC complex</b>	$\frac{d}{dt}w = b_w - X(r_{w21}R_X)w - (r_{w12}I_T + d_w)w$

As competitive binding alone was insufficient for the model to reproduce biological data, and negative regulation of *WER* by a *WER*/MYB23 complex co-localised regulatory network component was also insufficient, and *WER* had been shown not to positively regulate its own transcription [5,12], it was hypothesised that successful patterning may be achieved if *WER* transcription was repressed by a regulatory network component which dominated in trichoblast cells. The CPC complex was chosen and the repression of *WER* transcription by the CPC complex was tested.

For the model with *WER* translational repression by the cortical signal and CPC complex ten successful parameter sets were found out of the 20,000 tested, Figure 2B. The *WER* repression by CPC complex model could reproduce the nonuniform trichoblast spacing seen in WT and *scm* mutant root cross-sections, Figure 2C.

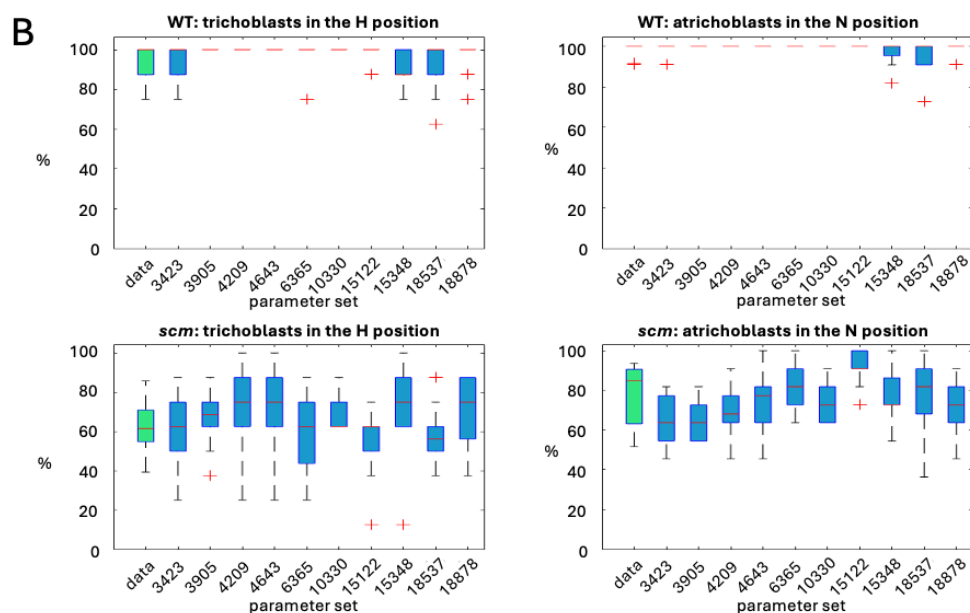
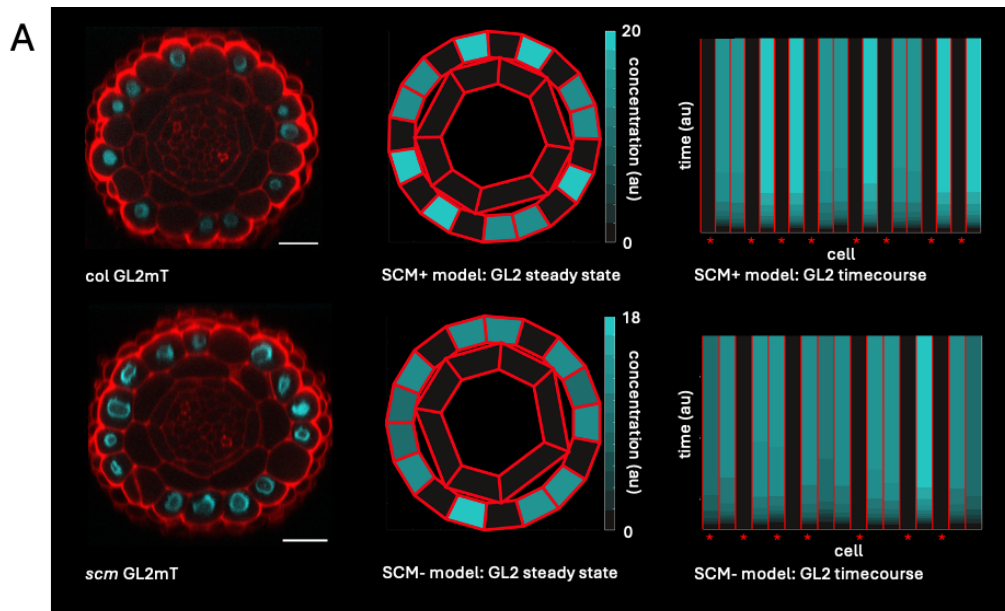


**Figure 2: Comparing results of the SCM+ and SCM- models, with *WER* transcriptional regulation by CPC complex, to data.** (A) Top row. Left, WT data. Middle, steady state solution of the SCM+ model, solved with parameter set  $P_{15348}$ . As the *WER*/*MYB* complex promotes *GL2* expression [7–9], the total *WER*/*MYB*23 complex concentration is used as a proxy for *GL2*. Right, model solution time course, stars on the horizontal axis show cortical cleft position. Bottom row has the same arrangement as the top row but for *scm* mutant data and SCM- model results. SCM- model was also solved with parameter set  $P_{15348}$ . (B) Box plots showing the distributions of percentages of trichoblast and atrichoblast cells counted in H and N positions. The first boxplot on each graph shows the distribution of the data. WT data was obtained from counting *GL2* expression in twenty-two root cross-sections (supplementary data). *scm* mutant data was obtained by counting eleven published longitudinal root images showing different markers (supplementary data). Each of the other boxplots contain results from twenty steady state solutions, each with a different random initial condition, for SCM+ and SCM- models, solved with parameter set shown.

The ten successful parameter sets did not occupy a common area of parameter space, nor could we find relationships within those ten successful parameter sets which did not also hold for at least some of the 19,990 unsuccessful sets (supplemental data). For all models, solutions for parameter sets which failed could be homogeneous or contain concentration differences which did not pass the 10% threshold (Section 2.2), have well defined cell types (Section 2.2) but trichoblast arrangement did not match the data in Table 3, or have poorly defined cell types. Solutions for all parameter sets tested did reach steady state, no oscillators were found.

These results suggest that a currently unknown *WER* transcriptional regulation is present in the root epidermis. Here, modelling has shown that the unknown regulation could take the form of *WER* transcriptional repression by a regulatory network component colocalised with the CPC complex.

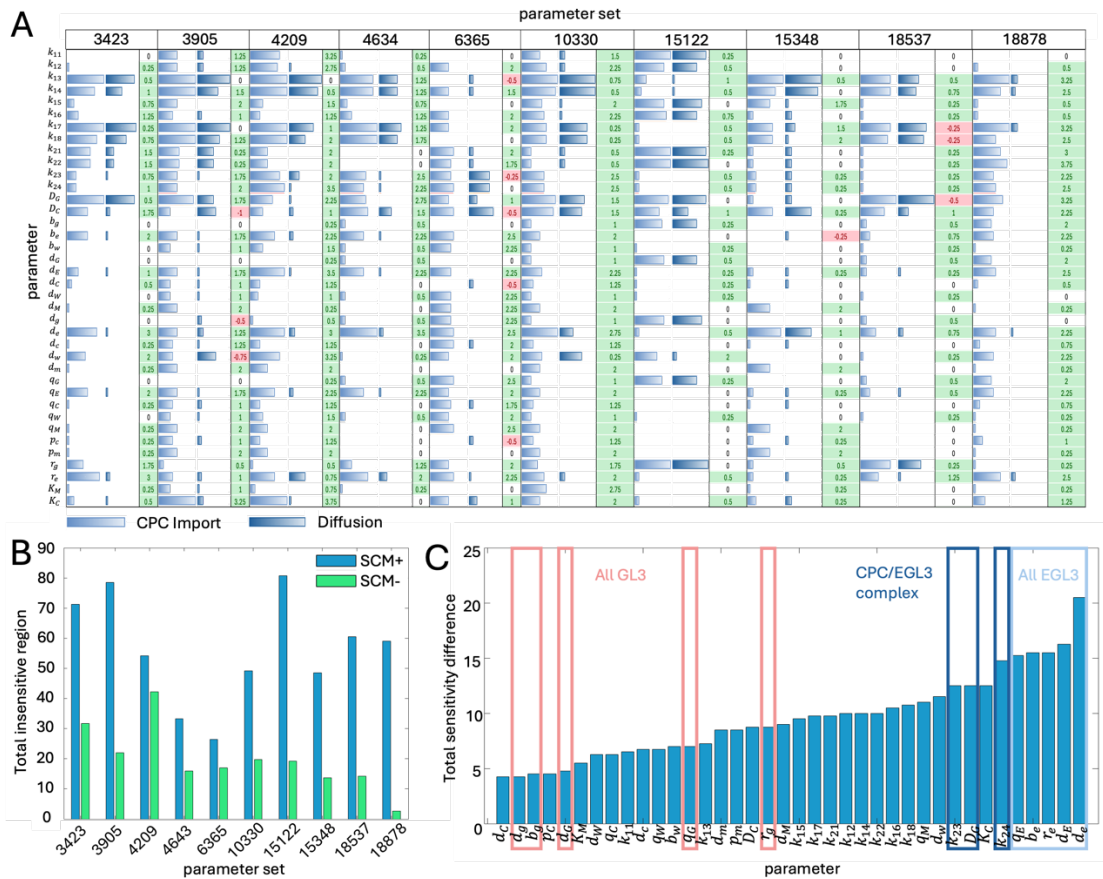
### **3.2 Dysregulation of CPC movement in the SCM- regulatory network model is sufficient to reproduce *scm* mutant data.**

For a parameter set to be labelled as a success, the parameter set must have reproduced *scm* mutant data when SCM was removed from the model (Section 2.2). SCM was previously hypothesised to be a cortical signal receptor because its removal from the plant decoupled trichoblasts from the cortical cleft [16]. With SCM's redefined role as a CPC importer [11], it was not clear that the dysregulation of CPC movement in *scm* mutant roots is sufficient to reproduce *scm* mutant trichoblast, atrichoblast patterns. These modelling results show that it is indeed the case. The results show that trichoblast patterning can be decoupled from the cortical clefts without any change to the cortical signal or the cortical signal receptor, the decoupling is a result of CPC movement dysregulation alone, Figure 2.

### **3.3 SCM import of CPC reduces epidermal patterning sensitivity to reaction rate changes.**

CPC is predominantly translated and transcribed in epidermal cells occupying N positions [14,15], where it competes with WER/MYB23 to bind GL3, EGL3, thus preventing WER/MYB23 complex formation [6,9]. SCM import of CPC, from cells in the N positions to cells in the H positions, likely aids patterning by reducing the amount of CPC available to compete with WER and MYB23 for GL3, EGL3. Sensitivity analysis was performed on the ten successful parameter sets found when *WER* transcription was repressed by cortical signal and the CPC complex, in both SCM+ and SCM- models (Section 2.3). In SCM+ models CPC movement is governed by diffusion plus SCM import, in the SCM- models CPC movement is governed by diffusion only, Equations (10) and (11). Insensitive regions were calculated for all core parameters,  $P_{i,j}$ , for SCM+ and SCM- models. Insensitive regions for SCM+ and SCM- models were then compared to understand if CPC import by SCM decreases the regulatory network's sensitivity to reaction rate changes.

A measure to compare the sensitivity between SCM+ and SCM- models was to calculate the difference between insensitive regions of the SCM- and SCM+ models for each core parameter  $p_{i,j}$ . The SCM- insensitive region was subtracted from the SCM+ sensitive region for each parameter, thus the resulting number defined how much less sensitive to changes in parameter  $p_{i,j}$  the SCM+ model was when compared to the SCM- model, i.e. if the result was negative the SCM+ model, containing CPC import and diffusion, was more sensitive to changes in parameter  $p_{i,j}$  than the SCM- model, containing CPC diffusion only. Parameter sensitivity varied considerably between parameter sets, Figure 3A. For six of the ten parameter sets analysed, the SCM+ model was less sensitive than the SCM- model for all parameters,  $p_{i,j}$ . The other four parameter sets contained one, three or five, out of the thirty-eight, core parameters for which the SCM+ model was more sensitive than the SCM- model. Nonetheless, the total insensitive region for all ten parameter sets was greater for the SCM+ model than for the SCM- model, Figure 3B, indicating that SCM import of CPC increases the regulatory network's robustness against reaction rate changes.



into the model, Equations (6), (9) and (12) to (15). To investigate the contribution of each of the multiple binding site reactions to *Arabidopsis* root epidermal patterning, models containing the most up to date published reactions, i.e. SCM as a CPC importer and EGL3 restricted movement, Table 2, and each *WER* regulation mechanism, Tables 5 and 6, were solved with one, two and all three multiple binding site reactions removed, Table 7, for all 20,000 core parameter sets.

**Table 7. Mechanistic parameter intervals for the multiple binding site investigation.** Other parameter intervals are shown in Tables 1 and 2. For one multiple binding site reaction removed, the name of the removed binding site reaction is shown. For two multiple binding site reactions removed, the name of the remaining binding site reaction is shown.  $n_1$  and  $n_2$  are in the same reaction, *WER*/*MYB23* complex formation.

	number of multiple binding site reactions removed	0	1			2			3
			multiple binding site removed			multiple binding site remaining			
		all	<i>CPC</i>	<i>MYB23</i>	<i>WER</i> / <i>MYB23</i> complex	<i>CPC</i>	<i>MYB23</i>	<i>WER</i> / <i>MYB23</i> complex	none
$n_1$	GL3, EGL3 in complex	{2,3,4}	{2,3,4}	{2,3,4}	1	1	1	{2,3,4}	1
$n_2$	<i>WER</i> , <i>MYB23</i> in complex	{2,3,4}	{2,3,4}	{2,3,4}	1	1	1	{2,3,4}	1
$n_3$	<i>MYB23</i> translation	{2,3,4}	{2,3,4}	1	{2,3,4}	1	{2,3,4}	1	1
$n_4$	<i>CPC</i> translation	{2,3}	1	{2,3}	{2,3}	{2,3}	1	1	1

No successful parameter sets were found for models in which *WER* transcription was repressed by cortical signal alone, for any combination of multiple binding sites, Table 8. For the models where *WER* transcription was repressed by cortical signal and *CPC*, three successful parameter sets were found for the model where multiple binding sites were on the *MYB23* promotor only. For all the three successful parameter sets, the number of *WER* binding sites on the *MYB23* promotor was four.

For the *WER* transcriptional repression by cortical signal and *CPC* complex models, successful parameter sets were found for numerous multiple binding site combinations. A notable result was that when one multiple binding site reaction was removed, the removal of multiple binding sites on the *MYB23* promotor was the only single multiple binding site removal which resulted in fewer successful parameter sets, when compared to the model with all multiple binding site reactions. Furthermore, when only one multiple binding site reaction remained, the *MYB23* promotor was the only multiple binding site reaction which, when alone, resulted in more successful parameter sets being found, when compared to the model with all multiple binding site reactions, Table 8, Figure 4A. Taken together, these results suggested that multiple binding sites on the *MYB23* promotor is a key driver of *Arabidopsis* root hair patterning.

*MYB23* transcription is part of a positive feedback loop with the *WER*/*MYB23* complex, Figure 1B. The *WER*/*MYB23* complex promotes *MYB23* transcription [5], the translated *MYB23* can then bind *GL3*/*EGL3* to form the *WER*/*MYB23* complex. No successful parameter sets were found when all multiple binding site reactions were removed nor when only multiple binding sites on the *CPC* promotor remained. Successful parameter sets were found when multiple binding sites were only enabled on the *MYB23* promotor, Table 8, or *WER*/*MYB* complex formation reactions. Thus, a single multiple binding site reaction within the *MYB23* positive feedback loop was sufficient to enable successful patterning.

**Table 8. Numbers of successful parameter sets found in the multiple binding site investigation.** Deep blue shaded cell shows the ten successful parameter sets found for the model with *WER* transcriptional repression by the cortical signal and *CPC* complex. The removal of multiple binding sites on the *MYB23* promotor reduced the number of successful parameter sets found (red shaded cell compared to deep blue cell). Multiple binding sites on the *MYB23* promotor only increased the number of successful parameter sets found (red shaded cells compared to blue cells).

number of multiple binding site reactions removed	0	1			2			3
		multiple binding site removed			multiple binding site remaining			
	all	<i>CPC</i>	<i>MYB23</i>	<i>WER</i> / <i>MYB23</i> complex	<i>CPC</i>	<i>MYB23</i>	<i>WER</i> / <i>MYB23</i> complex	none
cortical signal only	0	0	0	0	0	0	0	0
cortical signal and <i>CPC</i>	0	0	0	0	0	3	0	0
cortical signal and <i>CPC</i> complex	10	11	4	12	0	14	8	0

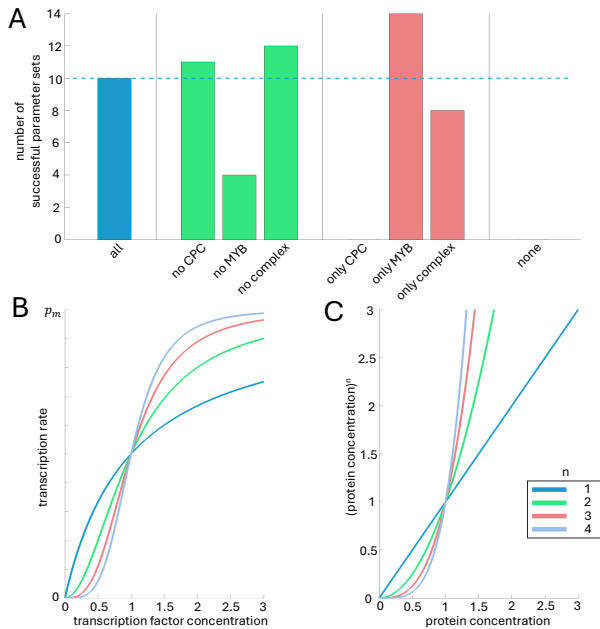


**Figure 4: Cooperativity and oligomerisation.** (A) The number of successful parameter sets found for model with *WER* transcription repressed by cortical signal and the CPC complex, for combinations of multiple binding site reactions (Tables 7 and 8). The blue bar shows the data when all three multiple binding sites are present, red bars show the data when only one multiple binding site reaction is removed, and yellow bars show the data when only one multiple binding site reaction remains. The dotted line is for comparison between the data for all three multiple binding sites are present and fewer than three multiple binding sites. (B) A graph showing how the transcription rate relates to transcription factor concentration, denoted  $[TF]$ , when transcription cooperativity within the promoter. Cooperativity shown  $n = \{1, 2, 3, 4\}$ . Formula,  $p_m [TF]^n (1 + [TF]^n)^{-1}$ , where  $p_m$  is the maximum transcription rate. (C) A graph showing the relationship between the rate of protein complex formation and the concentration of protein.

Having more than one binding site on the MYB23 promoter within the model,  $n_3 \in \{2, 3, 4\}$ , represents cooperativity between binding sites during transcriptional regulation.  $n_1 \in \{2, 3, 4\}$ ,  $n_2 \in \{2, 3, 4\}$  within the model represents oligomerisation within the WER/MYB23 complex. Mathematically, increasing cooperativity or the number of proteins within a complex, results in more pronounced nonlinearities, Figures 4B and 4C. Reactions with nonlinear dynamics, within biological systems can result in robustness against noise [31,32] and ultrasensitivity, depending largely on the value of  $n_i$ . For  $n_i > 1$ , a nonlinear reaction has a rate close to zero for small concentrations of regulatory proteins, i.e. the reaction is insensitive during periods when the regulatory protein concentrations are low. The insensitivity interval increases with  $n_i$ . For larger values of  $n_i$  nonlinear reactions take on an ultrasensitive, switch like, behaviour. Reaction insensitivity at low regulatory protein concentrations could be developmentally advantageous. Noise has a greater impact on the relative concentrations of regulatory proteins between cells when regulatory protein concentrations are low, thus reaction insensitivity at low regulatory protein concentrations would help to prevent noise from driving developmental patterning.

The WER/MYB23 complex is the central transcription factor complex controlling the concentrations of numerous regulatory network components during *Arabidopsis* root epidermal cell differentiation and thus root hair patterning. These modelling results suggest that multiple binding sites in reactions within the MYB23 positive feedback loop, particularly on *MYB23* translational regulation, are essential for correct root hair patterning. Their role may be two-fold, to protect the regulatory network from noise driven patterning early in development, and to create switch like dynamics when regulator concentrations pass some threshold.

### 3.5 Restricted EGL3 movement and CPC/EGL3 WER/GL3 preferential binding enable epidermal patterning.

EGL3 movement has been reported to be restricted when compared to the movement of GL3 [19]. In the models presented thus far, EGL3 has been unable to move between epidermal cells,  $D_E = 0$ . To understand if EGL3 restricted movement was necessary the models were solved with  $D_E > 0$ , Table 2, and each *WER* regulation mechanism, Tables 5 and 6, for all 20,000 core parameter sets. No successful parameter sets were found with  $D_E > 0$ , for models when *WER* transcription was repressed by cortical signal alone, or cortical signal plus CPC. Two successful parameter sets were found for *WER* transcription repressed by cortical signal and the CPC complex. One of the two successful core parameter sets for  $D_G > 0$  was also one of the ten successful parameter sets found when  $D_G = 0$ , core parameter set  $P_i = P_{4209}$ .

The diffusion coefficients of GL3 and EGL3 were compared for the two successful  $D_G > 0$  parameter sets. For both parameter sets, the diffusion coefficient of GL3 was greater than the diffusion coefficient of EGL3, Table 9, suggesting that, for successful *Arabidopsis* root epidermal patterning, EGL3 movement must be restricted compared to GL3 movement. To further test if EGL3 movement must be restricted compared to GL3 movement for successful patterning, the ten successful parameter sets found with  $D_E = 0$  were solved with  $D_E = D_G$ , all failed to reproduce experimental data, Table 3. Next the ten parameter sets were solved



with  $D_E = 10^{-\alpha} D_G$ , where  $\alpha = \{0.05, 0.1, 0.15, \dots, 3\}$  to find the maximum value of  $D_E$  which will enable patterning and the relationship between  $D_E$  and  $D_G$ . The largest value of  $D_E$  found to pattern successfully was denoted  $D_{E_{MAX}}$ , Table 9. All EGL3 diffusion coefficients,  $D_{E_{MAX}}$ , were less than the GL3 diffusion coefficient. The data suggests that EGL3 movement must be restricted compared to GL3 movement, for successful *Arabidopsis* root epidermal patterning.

**Table 9. GL3 and EGL3 diffusion coefficients.** GL3 diffusion coefficient,  $D_G$ , EGL3 diffusion coefficient,  $D_E$ , and the maximum EGL3 diffusion coefficient tested which enables successful patterning,  $D_{E_{MAX}}$ , for each parameter set,  $i$ , in the investigation.

$i$	4209	16189	$i$	3423	3905	4209	4634	6365	10330	15122	15348	16189	18537	18878
$D_G$	5.86	7.53	$D_G$	1.04	6.09	5.86	3.15	4.53	8.91	6.78	5.14	7.53	0.15	4.44
$D_E$	0.52	3.68	$D_{E_{MAX}}$	0.92	0.48	0.66	0.63	0	1.41	0.06	0.13	3.77	0.14	0.99
			$\alpha$	0.05	1.1	0.95	0.7	> 3	0.8	2.05	1.6	0.3	0.05	0.65

Both GL3 and EGL3 are translated and transcribed in trichoblast cells. The CPC concentration is greatest in trichoblast cells [17], which, in the model solutions, is due to the CPC complex dominating in these cells. The ability of GL3 to move more quickly from trichoblast to atrichoblast would be of limited use if the binding affinity between GL3 and CPC was greater than the binding affinity between EGL3 and CPC, as GL3 would become bound to CPC in trichoblast cells and unable to move. Furthermore, once in the atrichoblast cell, if the GL3 CPC binding affinity was greater than the GL3 WER/MYB23 binding affinities then CPC would become bound to GL3 and trapped in the atrichoblast cells. The binding affinity relationships were calculated for each successful parameter set, with  $D_E \geq 0$ , Table 10. It was found that eight out of eleven parameter sets,  $\approx 73\%$ , satisfied the relationship that CPC bound EGL3 more strongly than GL3. Seven out of eleven parameter sets,  $\approx 64\%$ , satisfied the relationship that WER bound GL3 more strongly than EGL3, and four,  $\approx 36\%$ , satisfied the relationship that MYB23 bound GL3 more strongly than EGL3. The results suggest that preferential binding of MYB23 with GL3 is less important than WER preferentially binding GL3. This is because during early development the WER complex dominates over the MYB23 complex in atrichoblast cells. The MYB23 promotor contains multiple WER binding sites [5] which means that the WER complex must become somewhat established before MYB23 is transcribed Figure 4B. Once MYB23 starts to be translated, the MYB23 positive feedback loop dominates in atrichoblast cells increasing the concentration of MYB23 such that the abundance alone is enough to sequester the majority GL3, enabling CPC to be imported into trichoblast cells.

**Table 10. Binding affinity ratios and the dominating complex in trichoblast and atrichoblast cells.** Data in the first three columns shows WER, MYB23 and CPC, GL3 binding affinity divided with WER, MYB23 and CPC, EGL3 binding affinity. If the ratio is less than 1 then the protein binds GL3 more strongly than EGL3, if the ratio is greater than 1 then the protein binds EGL3 more strongly than GL3. The complex which dominates in trichoblast and atrichoblast cells is also shown. Cells containing data that satisfies the relationships hypothesised as being optimal for epidermal patterning have been shaded in green.

$i$	WER	MYB23	CPC	dominating complex	
	$\frac{k_{12}k_{13}}{k_{11}k_{14}}$	$\frac{k_{16}k_{17}}{k_{15}k_{18}}$	$\frac{k_{22}k_{23}}{k_{21}k_{24}}$	trichoblast	atrichoblast
3423	0.40	0.02	37.78	CPC/EGL3	MYB23/GL3
3905	0.50	1.10	61.37	CPC/EGL3	MYB23/GL3
4209	0.04	2.04	1.07	CPC/GL3	MYB23/GL3
4634	5.48	1.47	0.44	CPC/GL3	MYB23/GL3
6365	4.72	11.01	0.49	CPC/GL3	MYB23/GL3
10330	0.06	1.95	1.72	CPC/EGL3	MYB23/GL3
15122	1.46	2.64	9.47	CPC/EGL3	MYB23/EGL3
15348	0.41	382.31	2.81	CPC/EGL3	MYB23/GL3
16189	0.94	0.09	17.37	CPC/EGL3	MYB23/GL3
18537	1.08	0.45	4.39	CPC/EGL3	MYB23/GL3
18878	0.33	0.23	119.62	CPC/EGL3	MYB23/GL3

The GL3 and EGL3 diffusion coefficients and binding affinity ratio analysis suggested that the CPC/EGL3 complex should be the most abundant complex in the trichoblast cells, and WER/GL3 and MYB23/GL3 complexes should be the most abundant complexes in atrichoblast cells. For a parameter set to have been

considered successful, the SCM+ and SCM- models were solved with twenty noisy initial conditions and the solutions of both models matched the biological data (Section 2.2). Thus, for each of the successful parameter sets, there were twenty SCM+ solutions and twenty SCM- solutions. The concentrations of complexes CPC/GL3, CPC/EGL3, WER/GL3, WER/EGL3, MYB23/GL3, MYB23/EGL3, for all 220 SCM+ steady state solutions were plotted, Figure 5A. It was the case that, when all solutions were considered together, CPC/EGL3 was more abundant than CPC/GL3 in trichoblast cells and WER/GL3, MYB23/GL3 were more abundant than WER/EGL3, MYB23/EGL3 in atrichoblast cells. The dominant complex in trichoblast cells was CPC/EGL3 giving insight as to why the sensitivity analysis performed in Section 3.3, Figure 3C, found that the removal of SCM import of CPC increased the network's sensitivity to changes in reaction rates related to CPC/EGL3 complex concentrations and not reaction rates related to GL3/CPC complex concentrations. The dominant complex in atrichoblast cells was the MYB23/GL3 complex, further illustrating the importance of the MYB23 positive feedback loop in epidermal patterning. The MYB23 complex was absent from trichoblast cells but the WER/GL3 complex was present in trichoblast cells in small amounts. This data illustrates why cooperativity between WER binding sites on the *MYB23* promotor is important for successful epidermal patterning, for low concentrations of WER complex *MYB23* will not be transcribed and the MYB23 positive feedback loop will not become established in trichoblast cells, Section 3.4, Figure 4B.

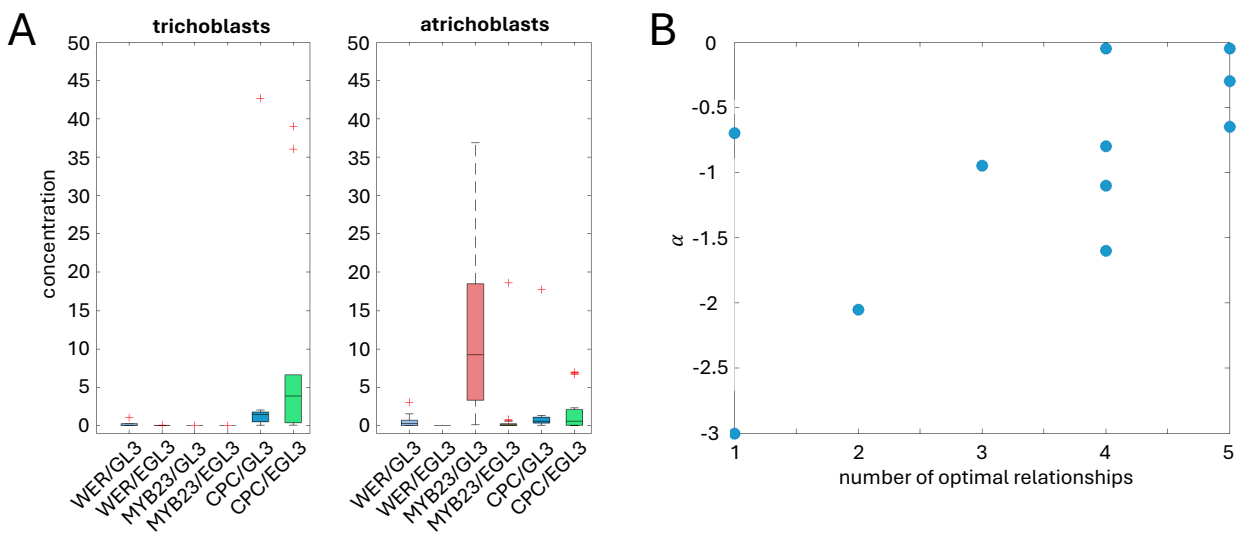


**Figure 5: EGL3 movement.** (A) Concentrations of protein complexes in trichoblast and atrichoblast cells, for all 220 SCM+ steady state solutions, with  $D_E = D_{E_{MAX}}$ , for the SCM+ model with *WER* translation regulated by the CPC complex and cortical signal. (B) Scatterplot showing the correlation between the number of optimal relationships a parameter set satisfied and the relationship between  $D_G$  and  $D_{E_{MAX}}$ .  $D_{E_{MAX}} = 10^{-\alpha} D_G$ . One data point per parameter set.

The complex concentrations for each of the twenty SCM+ solutions were also plotted for each of the eleven successful parameter sets individually, data not shown, and the complex which dominated in the trichoblast and atrichoblast positions was recorded, Table 10. It was found that for eight parameter sets,  $\approx 73\%$ , CPC/EGL3 was the dominating complex in trichoblast cells and for ten parameter sets,  $\approx 91\%$ , MYB23/GL3 was the dominating complex in atrichoblast cells. There were no successful parameter sets for which CPC/GL3 dominated in trichoblast cells and MYB23/EGL3 dominated in atrichoblast cells, demonstrating that at least one dominating complex had to be in the form optimal for epidermal patterning.

All the relationships hypothesised as being optimal for epidermal patterning were only satisfied by three parameter sets,  $\approx 27\%$ , and two parameter sets only satisfied one optimal relationship,  $\approx 18\%$ , Table 10. As there was no clear relationship between GL3 and maximum EGL3 diffusion coefficients, Table 9, it was asked if the order of magnitude difference between GL3 and EGL3 diffusion was correlated with the number of optimal relationships satisfied by each parameter set. The hypothesis was that the more optimal relationships a successful parameter set satisfied the closer to zero the value of  $-\alpha$  would be, i.e. the value of  $D_{E_{MAX}}$  would approach  $D_G$ . Indeed, the number of optimal relationships satisfied was found to correlate with  $-\alpha$ , with a correlation coefficient of 0.67 which was calculated to be statistically significant with p-value 0.02, Figure 5B.

Collectively these data show that restricted movement of EGL3, compared to GL3, is essential for correct epidermal patterning. How much slower than GL3 movement, EGL3 movement must be, is dependent on

other parameters within the regulatory network. If other parameters are set such that they aid the accumulation of CPC/EGL3 in trichoblast cells and WER/GL3, MYB23/GL3 in atrichoblast cells, then proper epidermal patterning is achieved with higher EGL3 diffusion coefficients.

## 4 Discussion

The work presented here uses mathematical modelling to integrate a wealth of experimental data into one regulatory network model. The system under scrutiny was the regulatory network governing cell fate determination in the *Arabidopsis* root epidermis. The root epidermal cell fate network contains a central regulation complex whose regulation is determined by one positive feedback loop, two negative feedback loops, cell-cell signalling within the epidermal tissue, and positional cues from the underlying tissue.

A lot is known about components of the regulatory network, how they interact, and the effect of component removal on *Arabidopsis* root hair patterning. However, the complexity of the network has made it difficult to understand the contributions of individual components, and reactions, to the networks overall ability to control epidermal patterning.

The work here aimed to bridge that gap. The model was built to have a one-to-one relationship with the regulatory network as we currently understand it. Numerous mechanistic investigations were performed using the model. The investigations were designed to test; the sufficiency of our current knowledge to reproduce wild type and mutant data, the necessity for cooperativity and oligomerisation within reactions, reaction rate relationships, and the impact on patterning of cell-cell signalling properties.

### 4.1 Results summary

Modelling results suggest that our current understanding of *WER* transcriptional regulation is incomplete. No successful parameter sets could be found for the model containing *WER* transcriptional regulation mechanisms supported by experimental data [12,9]. An obvious candidate for *WER* regulation would be for *WER* to promote its own transcription within atrichoblast cells, like *MYB23*, but this has already been shown not to be the case [12,5]. Thus, it was hypothesised that successful patterning may be achieved if *WER* transcription was repressed by a regulatory network component which dominates in trichoblast cells. As the CPC complex is a transcription factor complex, the CPC complex was chosen. The addition of *WER* transcriptional repression by the CPC complex enabled successful parameter sets to be found. As *WER* regulation by the CPC complex was a hypothesised regulation, all further mechanistic investigations were carried out in the models with published *WER* regulation and hypothesised *WER* regulation. For all but one of the subsequent investigations, the model with *WER* regulation by the CPC complex was the only model for which successful parameter sets could be found.

In recent years the role of SCM has been revised. Initially SCM was hypothesised to be a cortical signal receptor because its removal from the plant decoupled trichoblasts from the cortical cleft [16]. SCM has since been shown to function as a CPC importer [11]. It was easy to understand how the removal of a cortical signal receptor could decouple epidermal patterning from its positional cues. However, it was not obvious that removing CPC import from the regulatory network, while leaving cortical signal receptors and positional cues intact, would produce an epidermal pattern which appeared to be positional signalling impaired. Here, it was shown that the removal of CPC import from the regulatory network was sufficient to reproduce *scm* mutant data.

The import of CPC by SCM was shown to make the regulatory network's ability to reproduce biological data more robust against changes in reaction rates, when compared to the regulatory network within which CPC movement was governed by diffusion alone. These results confirm that the directed removal of CPC from cells in the N position is beneficial for the *WER*/*MYB23* complex to become established as the dominant complex in the N positions, and for the CPC complex to dominate in the H positions.

The *WER*/*MYB23* complex promotes the transcription of *CPC* and *MYB23* [14,15,5]. Multiple *WER* binding sites have been shown to exist on the *CPC* and *MYB23* promoters. The formation of the *WER*/*MYB23* complex also involves multiple binding site reactions and it is predicted that more than one of the *WER*, *MYB23*, *GL3* and *EGL3* proteins come together to form the complex [9]. The question of how multiple binding site reactions contributed to successful epidermal patterning was addressed. No benefit to successful patterning could be found for cooperativity on *CPC* transcriptional regulation. It was found that a multiple

binding site reaction within the MYB23 positive feedback loop was essential for the regulatory network to reproduce biological data, and that cooperativity on *MYB23* transcription contributed more to successful patterning than WER/MYB23 complex oligomerisation. Cooperativity within transcription and oligomerisation result in reaction dynamics whereby reactions are insensitive for low concentrations of reactants and highly sensitive for reactant concentrations past some threshold. These results suggest that for the *Arabidopsis* root epidermis to pattern successfully the positive feedback loop which amplifies the concentration of the central regulatory complex, the WER/MYB23 complex, must be protected against noise driven patterning early in development, and have switch like dynamics which enable WER/MYB complex domination when regulator concentrations pass some threshold.

GL3 and EGL3 are predominantly translated in trichoblast cells [6]. GL3 has been shown to move into atrichoblast cells, where it accumulates [13], whereas EGL3 remains in the trichoblast cells [19]. The necessity of GL3, EGL3 differential movement was investigated and found to be essential for the regulatory network model to reproduce data. It was found that the regulatory network could reproduce root hair patterning when EGL3 was able to diffuse between cells, however the diffusion coefficient of EGL3 had to be less than the diffusion coefficient of GL3, how much less depended on other parameters within the network. Parameter and steady state concentration relationships favourable for correct patterning were defined. Namely, CPC preferentially binds EGL3 during complex formation, WER and MYB23 preferentially bind GL3 during complex formation, CPC/GL3 is the dominant complex in trichoblast cells and MYB23/GL3 is the dominant complex in atrichoblast cells. The more favourable relationships satisfied, the smaller the difference between GL3 and EGL3 movement could be while still allowing the regulatory network to reproduce patterning data.

## 4.2 An integrated understanding

The results of the work presented give an integrated understanding of how the components and reactions within the *Arabidopsis* root epidermal regulatory network come together to ensure robust root hair patterning. Identical epidermal cells emerge from the root apical meristem. The identical cells start to transcribe *WER*, *GL3* and *EGL3*. A positional cue reduces the transcription of *WER* in epidermal cells occupying the H positions, distinguishing H position and N position cells. Thus, cells in the N position start to translate more WER and form more WER complex than cells in the H positions. An abundance of WER complex in N position cells reduces *GL3* and *EGL3* transcription. For the WER complex to remain dominant in the N positions WER must bind GL3 which has diffused into N position cells from the H positions. EGL3 movement is restricted so the majority of EGL3 remains in H position cells.

Cooperativity between WER binding sites on the *CPC* and *MYB23* promoters dictates that the WER complex concentration must build up before the WER complex starts to effectively promote *CPC* and *MYB23* translation. The initial insensitivity of the regulatory network to changes in WER complex concentration is essential to protect epidermal patterning from noise driven WER complex concentration changes early in development, when WER complex concentrations are low. Once *MYB23* transcription begins, the MYB23 positive feedback loop is activated and MYB23 complex concentrations increase dramatically. The abundance of MYB23 in N position cells sequesters GL3, and any EGL3, to make the MYB23 complex the dominant atrichoblast complex. WER becomes redundant after the initial developmental phase. Thus, the role of WER appears to be to receive positional cues during early development, with these positional cues transmitted through WER becoming ineffective later in development.

The promotion of *CPC* transcription by the WER/MYB complex leads to an abundance of CPC in N position cells. CPC can also form a complex with GL3 and EGL3 and thus competes with WER and MYB for GL3/EGL3 binding. To counteract the accumulation of CPC in the N positions, CPC is imported into H position cells from neighbouring N position cells. CPC has a stronger affinity to EGL3 than GL3. The preferential binding of EGL3 and CPC leaves GL3 unbound and free to diffuse from the H position cells into N position cells, where GL3 can be used to maintain high WER/MYB complex concentrations.

This work hypothesises that for the regulatory network to reproduce WT and *scm* mutant root epidermal patterning, the CPC complex, or another, unknown, regulatory network component that colocalises with the CPC complex, must inhibit *WER* translation to ensure that WER complex concentration does not increase to levels which would enable it to initiate the MYB23 positive feedback loop.

# Acknowledgements

Funded by the Leverhulme Project Grant RPG-2021-053.

## References

1. Dolan L, Duckett CM, Grierson C, Linstead P, Schneider K, Lawson E, Dean C, Poethig S, Roberts K. Clonal relationships and cell patterning in the root epidermis of *Arabidopsis*. *Development*. 1994 Sep 1;120(9):2465–74.
2. Galway ME, Masucci JD, Lloyd AM, Walbot V, Davis RW, Schiefelbein JW. The TTG Gene Is Required to Specify Epidermal Cell Fate and Cell Patterning in the Arabidopsis Root. *Dev Biol*. 1994 Dec 1;166(2):740–54.
3. Berger F, Haseloff J, Schiefelbein J, Dolan L. Positional information in root epidermis is defined during embryogenesis and acts in domains with strict boundaries. *Curr Biol*. 1998 Mar;8:421–30.
4. Lee MM, Schiefelbein J. WEREWOLF, a MYB-Related Protein in Arabidopsis, Is a Position-Dependent Regulator of Epidermal Cell Patterning. *Cell*. 1999 Nov;99(5):473–83.
5. Kang YH, Kirik V, Hulskamp M, Nam KH, Hagely K, Lee MM, Schiefelbein J. The *MYB23* Gene Provides a Positive Feedback Loop for Cell Fate Specification in the *Arabidopsis* Root Epidermis. *Plant Cell*. 2009 May 22;21(4):1080–94.
6. Bernhardt C, Lee MM, Gonzalez A, Zhang F, Lloyd A, Schiefelbein J. The bHLH genes *GLABRA3 (GL3)* and *ENHANCER OF GLABRA3 (EGL3)* specify epidermal cell fate in the *Arabidopsis* root. *Development*. 2003 Dec 29;130(26):6431–9.
7. Di Cristina M, Sessa G, Dolan L, Linstead P, Baima S, Ruberti I, Morelli G. The *Arabidopsis* Athb-10 (*GLABRA2*) is an HD-Zip protein required for regulation of root hair development. *Plant J*. 1996 Sep;10(3):393–402.
8. Masucci JD, Rerie WG, Foreman DR, Zhang M, Galway ME, Marks MD, Schiefelbein JW. The homeobox gene *GLABRA 2* is required for position-dependent cell differentiation in the root epidermis of *Arabidopsis thaliana*. *Development*. 1996 Apr 1;122(4):1253–60.
9. Song SK, Ryu KH, Kang YH, Song JH, Cho YH, Yoo SD, Schiefelbein J, Lee MM. Cell Fate in the Arabidopsis Root Epidermis Is Determined by Competition between WEREWOLF and CAPRICE. *Plant Physiol*. 2011 Nov 3;157(3):1196–208.
10. Kwak SH, Schiefelbein J. The role of the SCRAMBLED receptor-like kinase in patterning the Arabidopsis root epidermis. *Dev Biol*. 2007 Feb;302(1):118–31.
11. Song JH, Kwak SH, Nam KH, Schiefelbein J, Lee MM. QUIRKY regulates root epidermal cell patterning through stabilizing SCRAMBLED to control CAPRICE movement in Arabidopsis. *Nat Commun*. 2019 Apr 15;10(1):1744.
12. Savage NS, Walker T, Wieckowski Y, Schiefelbein J, Dolan L, Monk NAM. A Mutual Support Mechanism through Intercellular Movement of CAPRICE and GLABRA3 Can Pattern the Arabidopsis Root Epidermis. Weigel D, editor. *PLoS Biol*. 2008 Sep 23;6(9):e235.
13. Bernhardt C, Zhao M, Gonzalez A, Lloyd A, Schiefelbein J. The bHLH genes *GL3* and *EGL3* participate in an intercellular regulatory circuit that controls cell patterning in the *Arabidopsis* root epidermis. *Development*. 2005 Jan 15;132(2):291–8.
14. Koshino-Kimura Y, Wada T, Tachibana T, Tsugeki R, Ishiguro S, Okada K. Regulation of CAPRICE Transcription by MYB Proteins for Root Epidermis Differentiation in Arabidopsis. *Plant Cell Physiol*. 2005 Jun 1;46(6):817–26.

15. Ryu KH, Kang YH, Park Y hwan, Hwang I, Schiefelbein J, Lee MM. The WEREWOLF MYB protein directly regulates *CAPRICE* transcription during cell fate specification in the *Arabidopsis* root epidermis. *Development*. 2005 Nov 1;132(21):4765–75.
16. Kwak SH, Shen R, Schiefelbein J. Positional Signaling Mediated by a Receptor-like Kinase in *Arabidopsis*. *Science*. 2005 Feb 18;307(5712):1111–3.
17. Kurata T, Ishida T, Kawabata-Awai C, Noguchi M, Hattori S, Sano R, Nagasaka R, Tominaga R, Koshino-Kimura Y, Kato T, Sato S, Tabata S, Okada K, Wada T. Cell-to-cell movement of the CAPRICE protein in *Arabidopsis* root epidermal cell differentiation.
18. Kwak SH, Schiefelbein J. A Feedback Mechanism Controlling SCRAMBLED Receptor Accumulation and Cell-Type Pattern in *Arabidopsis*. *Curr Biol*. 2008 Dec;18(24):1949–54.
19. Kang YH, Song SK, Schiefelbein J, Lee MM. Nuclear Trapping Controls the Position-Dependent Localization of CAPRICE in the Root Epidermis of *Arabidopsis*. *Plant Physiol*. 2013 Sep;163(1):193–204.
20. Benítez M, Espinosa-Soto C, Padilla-Longoria P, Alvarez-Buylla ER. Interlinked nonlinear subnetworks underlie the formation of robust cellular patterns in *Arabidopsis* epidermis: a dynamic spatial model. *BMC Syst Biol*. 2008 Dec;2(1):98.
21. Hill AV. The combinations of haemoglobin with oxygen and with carbon monoxide. *Proc Physiol*. 1910 Jan 22;40:iv–vii.
22. Weiss JN. The Hill equation revisited: uses and misuses. *FASEB J*. 1997 Sep;11(11):835–41.
23. Song et al. - 2011 - Cell Fate in the *Arabidopsis* Root Epidermis Is Det.pdf.
24. Kwak SH, Woo S, Lee MM, Schiefelbein J. Distinct Signaling Mechanisms in Multiple Developmental Pathways by the SCRAMBLED Receptor of *Arabidopsis*. *PLANT Physiol*. 2014 Oct 1;166(2):976–87.
25. Chaudhary A, Chen X, Leśniewska B, Boikine R, Gao J, Wolf S, Schneitz K. Cell wall damage attenuates root hair patterning and tissue morphogenesis mediated by the receptor kinase STRUBBELIG. *Development*. 2021 Jul 15;148(14):dev199425.
26. Lampropoulos A, Sutikovic Z, Wenzl C, Maegele I, Lohmann JU, Forner J. GreenGate - A Novel, Versatile, and Efficient Cloning System for Plant Transgenesis. Janssen PJ, editor. *PLoS ONE*. 2013 Dec 20;8(12):e83043.
27. Kumpers BMC, Han J, Vaughan-Hirsch J, Redman N, Ware A, Atkinson JA, Leftley N, Janes G, Castiglione G, Tarr PT, Pyke K, Voß U, Wells DM, Bishopp A. Dual expression and anatomy lines allow simultaneous visualization of gene expression and anatomy. *Plant Physiol*. 2022 Jan 20;188(1):56–69.
28. Zhang X, Henriques R, Lin SS, Niu QW, Chua NH. *Agrobacterium*-mediated transformation of *Arabidopsis thaliana* using the floral dip method. *Nat Protoc*. 2006 Aug;1(2):641–6.
29. Kurihara D, Mizuta Y, Sato Y, Higashiyama T. ClearSee: a rapid optical clearing reagent for whole-plant fluorescence imaging. *Development*. 2015 Jan 1;dev.127613.
30. Ursache R, Andersen TG, Marhavý P, Geldner N. A protocol for combining fluorescent proteins with histological stains for diverse cell wall components. *Plant J*. 2018 Jan;93(2):399–412.
31. Green RM, Fish JL, Young NM, Smith FJ, Roberts B, Dolan K, Choi I, Leach CL, Gordon P, Cheverud JM, Roseman CC, Williams TJ, Marcucio RS, Hallgrímsson B. Developmental nonlinearity drives phenotypic robustness. *Nat Commun*. 2017 Dec 6;8(1):1970.
32. Steinacher A, Bates DG, Akman OE, Soyer OS. Nonlinear Dynamics in Gene Regulation Promote Robustness and Evolvability of Gene Expression Levels. Proulx SR, editor. *PLOS ONE*. 2016 Apr 15;11(4):e0153295.

